# Association of Microaneurysms on Adaptive Optics Scanning Laser Ophthalmoscopy With Surrounding Neuroretinal Pathology and Visual Function in Diabetes

Jan Lammer,[1,2] Sonja G. Karst,[1,2] Michael M. Lin,[1,3] Michael Cheney,[1] Paolo S. Silva,[1,3] Stephen A. Burns,[4] Lloyd Paul Aiello,[1,3] and Jennifer K. Sun[1,3]

[1]Beetham Eye Institute, Joslin Diabetes Center, Boston, Massachusetts, United States
[2]Department of Ophthalmology and Optometry, Medical University Vienna, Vienna, Austria
[3]Department of Ophthalmology, Harvard Medical School, Boston, Massachusetts, United States
[4]School of Optometry, Indiana University, Bloomington, Indiana, United States

Correspondence: Jennifer K. Sun, Beetham Eye Institute, Joslin Diabetes Center, One Joslin Place, Boston, MA 02215, USA; jennifer.sun@joslin.harvard.edu.

Submitted: April 3, 2018
Accepted: September 13, 2018

Citation: Lammer J, Karst SG, Lin MM, et al. Association of microaneurysms on adaptive optics scanning laser ophthalmoscopy with surrounding neuroretinal pathology and visual function in diabetes. *Invest Ophthalmol Vis Sci*. 2018;59:5633–5640. https://doi.org/10.1167/iovs.18-24386

**Purpose.** We evaluate diabetic microaneurysm (MA) features on high-resolution adaptive optics scanning laser ophthalmoscopy (AOSLO) and their correlations with visual acuity (VA) and local retinal pathology on spectral domain optical coherence tomography (SDOCT).

**Methods.** Diabetic participants underwent VA testing and AOSLO and SDOCT imaging of MAs. AOSLO images were graded for MA dimension, wall hyperreflectivity (WH), intraluminal hyperreflectivity (IH), and perfusion pattern. SDOCTs centered on each MA were graded for disorganization of the retinal inner layers (DRIL) and other neuroretinal pathology.

**Results.** We imaged 109 MAs (30 eyes). Multivariate modeling, including statistically significant covariates from bivariate analyses, associated WH with greater MA size ($P = 0.001$) and DRIL ($P = 0.04$). IH was associated with perfusion ($P = 0.003$) and MA visibility on photographs ($P = 0.0001$), and larger MA size with partial perfusion ($P = 0.03$), MA ring signs ($P = 0.0002$), and photographic visibility ($P = 0.01$). Multivariate modeling revealed an association of WH and VA with DRIL.

**Conclusions.** AOSLO imaging demonstrates associations of hyperreflective MA walls with MA size and adjacent DRIL, as well as the presence of DRIL with lower VA. This study identifies a correlation between vascular and neural pathology associated with VA decline. Further studies of MA structure and neuroretinal disorganization may enable novel approaches to assess anatomic and functional outcomes in the diabetic eye.

Keywords: diabetic retinopathy, DR, microaneuryms, MA, retina, optical coherence tomography, OCT, adaptive optics scanning laser ophthalmoscope, AOSLO

The onset of clinically visible microaneurysms (MA) is an early hallmark of diabetic retinopathy (DR). Indeed, extent and severity of MAs in an individual eye are used to determine DR severity and strongly correlate with subsequent disease progression.[1–3]

Ex vivo histopathologic studies from animal models and human specimens have shown that selective loss of pericytes in retinal capillaries precedes the appearance of MAs. The weakened vessel wall support in areas of profound pericyte loss may lead to MAs of the capillary wall, which commonly are associated with endothelial cell alterations, basement membrane thickening, and lumen clotting.[4–8] In addition, leakage of fluid from capillaries and MAs is a primary mechanism for the onset and progression of diabetic macular edema (DME), one of the most common causes of vision loss in diabetic individuals. However, neither histopathologic studies nor current standard in vivo imaging modalities, such as color fundus photography and fluorescein angiography, allow the dynamic characterization of MAs at the cellular level in humans.

The advent of adaptive optics scanning laser ophthalmoscopy (AOSLO), which provides noninvasive, high-resolution retinal imaging, enables evaluation of the living human retinal vasculature at the cellular level. Adaptive optics systems correct more than 90% of the wavefront aberrations from an individual eye through the coupling of a wavefront sensor with a control system that achieves aberration compensation through deformable mirror technology, enabling a transverse resolution limit of approximately 2 μm.[9–11] Using AOSLO, dynamic and static imaging of the human retinal vasculature became feasible, providing insight into the vascular wall microstructure as well as flow dynamics within the vascular tree.[12–23]

AOSLO imaging combined with commercially available spectral domain optical coherence tomography (SDOCT) enables an added understanding of the retinal neurovascular unit as a whole, since SDOCT provides axial resolution of approximately 5 μm and can resolve individual retinal neural layers in the healthy and diseased states.[24] Thus, SDOCT imaging provides complementary characterization of the neural tissue surrounding specific MAs, including the presence of adjacent intraretinal cysts, disorganization of the retinal layers, or changes to overall retinal thickness adjacent to the MA.[25,26]

We performed AOSLO and SDOCT imaging of individual retinal MAs and the local surrounding neural retina in persons with diabetes to determine if structural or physiologic AOSLO

MA characteristics correlate with local retinal neural pathology on SDOCT. We also assessed if MA parameters evaluated on AOSLO are associated with altered local retinal visual function within the central macula.

## Materials and Methods

The study was approved by the Joslin Diabetes Center institutional review board and adhered to the tenets of the Declaration of Helsinki. Before enrollment and the performance of any study procedures, written informed consent was obtained from each participant.

### Patients and Examination

Patients were recruited for this study from regularly scheduled retina clinics at the Beetham Eye Institute of Joslin Diabetes Center, a tertiary care referral center specializing in diabetic eye disease. Patients were eligible to participate if they met the following inclusion criteria: minimum age 18 years, diagnosis of type 1 or type 2 diabetes, clear optical media (cornea, lens, vitreous), and stable central fixation. Patients with substantial media opacities precluding good quality imaging or retinal pathology due to nondiabetic diseases were excluded from study participation.

During a single study visit, all participants underwent a comprehensive, dilated ophthalmologic evaluation, including Early Treatment Diabetic Retinopathy Study (ETDRS)–protocol procedures of both eyes: refraction, best-corrected visual acuity (BCVA), and modified 7-field color fundus photography (FF4 Fundus Camera; Carl Zeiss Meditec, Inc., Dublin, CA, USA). Additionally, AOSLO and SDOCT imaging (Spectralis OCT; Heidelberg Engineering, Heidelberg, Germany) was performed. DR severity based on the ETDRS DR severity scale for each eye was determined by grading of color fundus photographs.[27] The SDOCT imaging protocol consisted of 49 B-scans (spacing between scans, 120 μm; high resolution mode, 16 frames Automated Real-Time Averaging [ART]), covering a field of $20^\circ \times 20^\circ$ centered at the fovea.

### Adaptive Optics Imaging and Image Post-Processing

The AOSLO (Boston Micromachines, Cambridge, MA, USA) used for this study was a subtype of the Indiana system that has been described previously.[28–30] In brief, the confocal SLO subsystem operates with a 13 nm imaging beam bandwidth centered at 830 nm. The AO subsystem uses a deformable mirror (Boston Micromachines) and a Shack-Hartman wavefront sensor (180 samples within a nominal pupil of 6.4 mm on the eye) controlled by custom software. The field size is approximately $1^\circ \times 1.2^\circ$ with a lateral resolution limit of 2.5 μm on the retina.

The retinal posterior pole was imaged by moving the scanning field stepwise across the $10^\circ \times 10^\circ$ retinal area centered at the fovea. MAs within this area were identified for AOSLO imaging based on fundus photos and SDOCT images. Additional outpouchings of the capillary walls not initially visible on fundus photos or SDOCT that were detected during AOSLO imaging sessions also were defined as MAs and included in the analysis. Imaging of MAs was performed by shifting focus between the retinal nerve fiber layer and RPE. Audio-video interleave (AVI)[31] files of up to 10 blocks were recorded of each MA at a rate of 30 frames per second. Each block consisted of 50 frames, and blocks were acquired at differing levels of focus that ranged through the anterior surface, central portion, and posterior surface of each MA as well as the nerve fiber layer anteriorly and photoreceptor layer posteriorly. Further image processing was performed using a customized software platform (written in MatLab; MathWorks, Natick, MA, USA). After dewarping AVI files to correct for sinusoidal distortion,[29] frames were semiautomatically selected and automatically aligned to generate averaged images and stabilized AVI files without motion artifacts, respectively. Each study eye's axial length was assessed using an IOL master (Carl Zeiss Meditec, Inc.) to reliably measure and quantify MA size (in μm) on the AOSLO images.

### Image Analysis

AOSLO images were registered to corresponding fundus photographs based on vascular landmarks and known imaging coordinates. For all MAs, visibility on fundus photography and infrared images was assessed and MAs were graded as visible or not visible on these imaging modalities. Eccentricity from the foveal center point also was calculated for each MA (Fig. 1).

AOSLO and SDOCT images were exported for further offline processing and analysis in Fiji (Fiji is Just ImageJ; National Institutes of Health [NIH], Bethesda, MD, USA).[32] The following variables were graded in a binary fashion on the high-resolution AOSLO videos: MA perfusion status (completely perfused versus partially perfused), presence of intraluminal hyperreflectivity (IH, present versus absent) and presence of MA wall hyperreflectivity (WH, present versus absent). WH was defined as any portion of increased pixel intensity along the MA wall compared to the remaining MA wall. Longest diameter of each MA was measured in μm. Perfusion was defined as visible flow of blood cells within the graded MA on AOSLO videos. IH was defined as hyperreflectivity within the MA lumen with a rough appearance and/or connection to the MA wall that also had adjacent blood cell flow near the IH. Smooth, centrally located hyperreflectivity with no local disturbances in blood flow was ascribed to lensing artifact due to the dome-shaped architecture of MAs, and was not included in the analysis (see Fig. 2).

For assessment of morphologic alterations of the neural retinal layers, SDOCT substacks of 5 B-scans centered on each MA were generated. Within each B scan, a 500 μm box centered on each MA was assessed for retinal volume, outer layer disruption, disorganization of retinal inner layers (DRIL),[33] intraretinal cysts, hyperreflective retinal spots,[34] and MA ring signs.[25] All SDOCT variables were graded in binary fashion as present versus absent on each B scan.

### Statistical Analysis

Associations between AOSLO parameters and SDOCT parameters were first assessed using nonparametric Wilcoxon rank sum or Fisher's exact test analyses treating results from each MA as an independent observation. To adjust for possible confounding, parameters that were statistically significant in these analyses then were included in mixed effects logistic regression models to determine the strength of the relationship between variables while adjusting for correlations between MAs from the same eye within 500 μm of each other. Statistical analyses were run in SAS (version 9.4; SAS Institute, Inc., Cary, NC, USA). The level of statistical significance was set at $P < 0.05$ for these exploratory analyses.

## Results

We studied 30 eyes of 29 individuals. Median (interquartile range [IQR]) age was 46 (37–57) years, and 11 (38%) were female. Of the participants, 22 (76%) had type 1 diabetes with

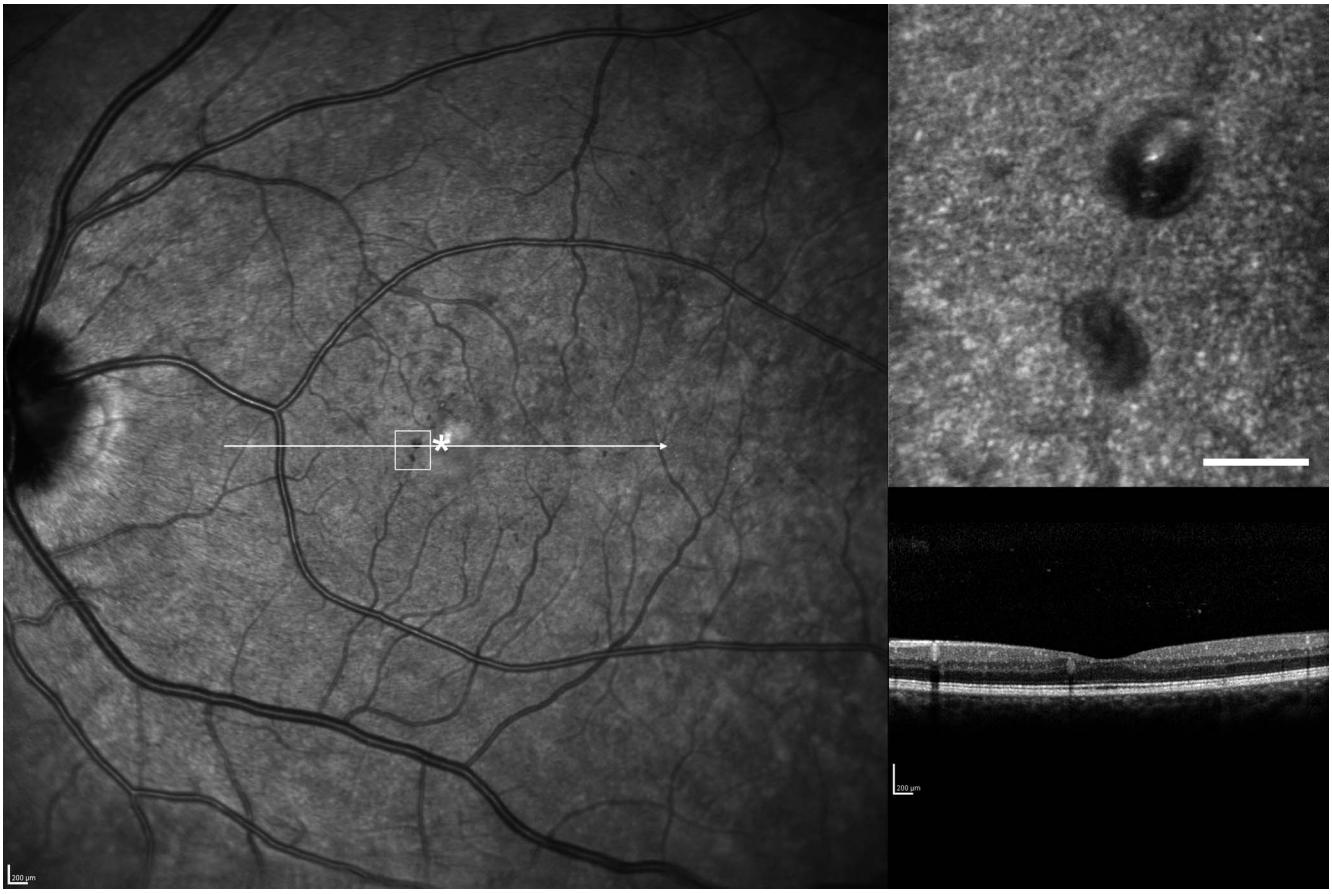

FIGURE 1. Registering of microaneurysms on AOSLO imaging with wider-field infrared (IR) and SDOCT images. The *white rectangle* in the IR image (*left*) indicates the location of the AOSLO scan (*upper right*), the *white horizontal line* the location of the SDOCT scan (*lower right*). *Scale bars*: in IR and SDOCT image = 200 μm; in AOSLO image = 100 μm. *Center of fovea.

a median (IQR) diabetes duration of 26 (18–32) years and hemoglobin A1c (HbA1c) of 7.7% (6.5%–8.4%). Median logMAR visual acuity (VA) in the study eyes was –0.04 (–0.10–0; Snellen equivalent of 20/20 +2 letters [20/25–20/20]). A detailed description of the study population characteristics is reported in Table 1.

## AOSLO MA Parameters Associations With Morphologic Alterations

A total of 109 MAs were imaged. In unadjusted, bivariate analyses, associations were found between the presence of WH using AOSLO imaging and longer MA dimension (WH present, 104.6 [75.9–129.1] μm versus no WH present, 50.0 [38.3–65.2] μm; $P < 0.0001$), the presence of intraluminal MA hyperreflectivity (WH present, 82.4% versus no WH, 33.3%; $P < 0.0001$), visible perfusion within MA (WH present, 76.5% versus no WH, 33.3%; $P < 0.0001$), DRIL (WH present, 14.7% versus no WH, 2.7%, $P = 0.03$), and visibility on fundus photography (WH present, 93.2% versus no WH, 59.1%; $P = 0.001$). No significant relationship with WH was found for sex, age, duration of diabetes, thickness, or volume of the ETDRS subfield of the respective MA, presence of intraretinal cysts ≥ 250 μm, MA ring signs, epiretinal membranes, hyperreflective retinal spots, or outer retinal layer disruption on SDOCT, or MA wall deformability as seen on AOSLO (Table 2).

The presence of IH found in AOSLO imaging was associated with shorter duration of diabetes (IH present, 26 [15–35] years versus no IH, 29 [17–42] years; $P = 0.047$), longer MA dimension (IH, 6.5 [59.2–119.0] μm versus no IH, 48.5 [35.1–65.6] μm; $P < 0.0001$), visible perfusion within each MA (IH, 79.3% [$n = 42$] versus no IH, 16.1% [$n = 9$]; $P < 0.0001$) and visibility on fundus photography (IH present, 95.9% [$n = 47$] versus no IH, 42.6% [$n = 20$]; $P < 0.0001$). No significant relationship was found with sex, age, thickness, or volume of the ETDRS subfield of the respective MA, presence of MA ring signs, intraretinal cysts, epiretinal membranes, hyperreflective retinal spots, outer retinal layer disruption or DRIL as seen on SDOCT, or MA wall deformability as seen on AOSLO (Table 2).

Larger MA size was associated with IH (MA < 61 μm, 30.9% versus. MA ≥ 61 μm, 66.7%; $P < 0.0003$), visible perfusion within each MA (MA < 61 μm, 25.5% versus MA ≥ 61 μm, 68.5%; $P < 0.0003$), MA ring sign on SDOCT (MA < 61 μm, 20.0% versus MA ≥ 61 μm, 60.5%; $P = 0.01$), and visibility on fundus photography (MA < 61 μm, 49.0% versus MA ≥ 61 μm, 93.3%; $P < 0.0001$). No significant relationship with MA size was found for sex, age, thickness, or volume of the ETDRS subfield of the respective MA, presence of intraretinal cysts ≥ 250 μm, epiretinal membranes, hyperreflective retinal spots, outer retinal layer disruption or DRIL on SDOCT, or MA wall deformability on AOSLO (Table 2).

Multivariable modeling was performed adjusting for all characteristics that were statistically significant in unadjusted analyses as well for correlations between MAs from the same eye within 500 μm of each other. For WH in AOSLO imaging, only MA dimension (point estimate [95% confidence limits], 0.04 [0.02, 0.07]; $P = 0.001$) and DRIL (1.29 [0.04, 2.53]; $P = 0.04$) remained associated. IH remained related to visible

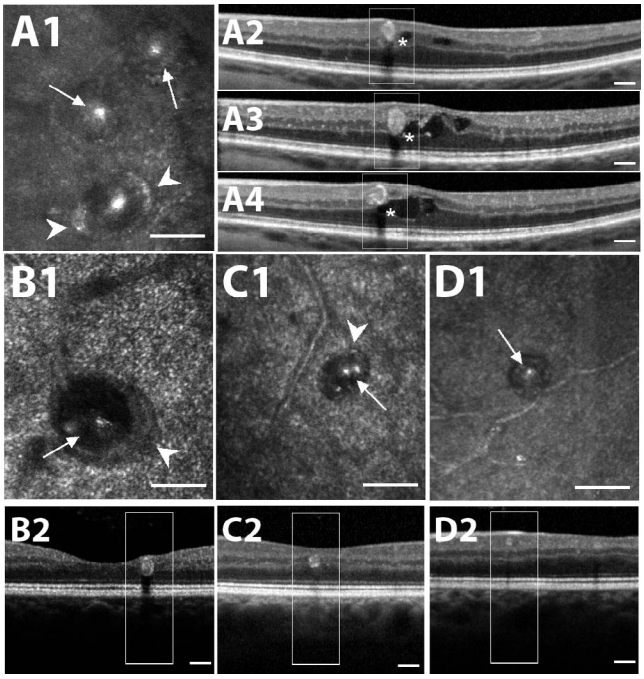


**Figure 2.** Examples of microaneurysms in AOSLO (**A1–D1**) and SDOCT imaging (**A2–4–D2**). *Arrowheads* indicate examples of hyperreflective walls, *arrows* indicate examples of IH at the center and wall. Note the rough structure of the IH in all examples (*arrows*), with IH connected to the MA wall in (**A1**), (**B1**), and (**C1**). The central, bright IHs in A1 are examples of lensing effects. See Discussion for details. (**A2–4–D2**) Corresponding SDOCT B-scans to respective AOSLO images. The *white box* indicates the 500 μm surrounding the microaneurysm. Note the proximity of intraretinal cysts (*asterisk* in [**A2–4**]) to the MA and the disorganization of retinal inner layers adjacent to/or caused by the respective MA (**A2–4–C2**). *Scale bars*: in AOSLO images (**A1–D1**) = 100 μm, in SDOCT images (**A–4–D2**) = 200 μm.

perfusion (2.33 [0.79, 3.87]; $P = 0.003$), and visibility on fundus photography (3.12 [1.66, 4.56]; $P < 0.0001$). For MA size, associations with visible perfusion (2.58 [0.32, 4.84]; $P = 0.03$), presence of MA ring signs on SDOCT (3.55 [1.71, 5.40]; $P = 0.0002$), and visibility on fundus photography (2.98 [0.76, 5.21]; $P = 0.01$) remained statistically significant (Fig. 3).

### AOSLO MA Characteristics and VA

To assess the relationship of AOSLO MA parameters with retinal function, the relationship between VA and AOSLO characteristics of MAs located within 500 μm of the foveal center ($n = 41$) was analyzed. In a bivariate analysis, the absence of WH was associated with better logMAR VA (–0.06 [–0.11, –0.01]; $P = 0.02$). Worse logMAR VA also was associated with larger MA diameter (0.001 [0.0005, 0.001]; $P = 0.001$) and presence of DRIL (0.17 [0.13, 0.19]; $P < 0.0001$). A multivariable model assessing the relationship between VA and WH, MA size, IH, and presence of DRIL found that only DRIL (0.13 [0.06, 0.19]; $P = 0.004$) remained associated with VA (Fig. 4).

## Discussion

In this cross-sectional exploratory study, we demonstrated that the combination of high resolution AOSLO imaging with SDOCT can provide detailed assessment of the in vivo interplay between vascular and neural pathology in the diabetic retina.

**Table 1.** Baseline Characteristics of the Study Population $n = 29$

| Characteristics | Value<br>Median (IQR); No. (%)* |
|---|---|
| Age, y | 46 (37–57) |
| Women | 11 (38%) |
| Diabetes | |
| Type I | 22 (76%) |
| HbA1c, % | 7.9 (6.5–8.4) |
| Type II | 7 (24%) |
| HbA1c, % | 6.4 (6.3–8.1) |
| Duration, y | 26 (18–32) |
| VA, logMAR | 0.04 (−0.10 to 0.00) |
| VA, Snellen equivalent | 20/20 +2 letters (20/25–20/20) |
| Axial length, mm | 23.54 (23.30–24.27) |
| Severity of DR | |
| Mild NPDR | 3 (10.3%) |
| Moderate NPDR | 8 (27.6%) |
| Severe NPDR | 7 (24.1%) |
| PDR | 10 (34.5%) |
| QPDR | 1 (3.5%) |

no., absolute numbers; NPDR, nonproliferative diabetic retinopathy; PDR, proliferative diabetic retinopathy; QPDR, quiescent proliferative diabetic retinopathy.

* Percentages may not sum up to 100.00% because of rounding.

Using these state-of-the-art imaging modalities, we were able to identify an association between specific AOSLO MA wall characteristics and neural disorganization and worse visual outcomes. Hyperreflectivity of MA walls on AOSLO is related to greater likelihood of local presence of neural disorganization as assessed by DRIL on SDOCT. This is important, since DRIL extent is associated with concurrent and predictive of future visual outcomes in eyes with DME.[33,35] Indeed, in this study, the presence of DRIL within 500 μm of the foveal center was significantly associated with worse VA.

The cause of wall hyperreflectivity on AOSLO has yet to be determined, although possible correlates are suggested by histopathology. Stitt et al.[5] proposed a classification of MA based on the integrity of pericytes, endothelial cells and the basement membrane, as well as the accumulation of cells within the MA lumen. Four different types were described ranging from loss of pericytes with preservation of endothelial cells (type I) to loss of pericytes and endothelial cells (type II and III), to late stages with loss of wall cells accompanied by an increase in basement membrane thickness (type III and IV). The significant association of MA WH on AOSLO with MA size in our data suggests that these MAs might represent later stage MAs that have grown in size and possibly progressed to increased basement membrane thickening. In this study, MA WH on AOSLO did not correlate with the presence of hyperreflective MA ring signs on SDOCT, suggesting that the two different imaging modalities are sensitive to different structural aspects of MA walls.

The hypothesis that MAs with WH are more mature and/or older is consistent with our results demonstrating that MA WH is significantly associated, not only with larger MA size, but also with presence of local neural retinal pathology. Foveal DRIL is a biomarker that is strongly correlated with current and future visual outcomes in eyes with DME. Greater extent of central retinal DRIL is associated with worse current VA in eyes with existing or resolved center-involved DME.[35] Furthermore, early 4-month change in DRIL extent is highly correlated with longer-term change in VA over 1 year, independent of changes in SDOCT central subfield thickness.[35] The developmental relationship between WH on AOSLO and DRIL on SDOCT has

TABLE 2. Unadjusted Analyses of Associations Between MA AOSLO Variables and Demographic and SDOCT Parameters, $n = 109$ MAs

| Variable | Wall Hyperreflectivity* Median IQR % (*n*) | | | Intraluminal Hyperreflectivity* Median IQR % (*n*) | | | MA Size* Median IQR % (*n*) | | |
|---|---|---|---|---|---|---|---|---|---|
| | Present | Absent | *P* Value | Present | Absent | *P* Value | <61 μm | ≥61 μm | *P* Value |
| Male sex | 76.5% (26) | 77.3% (58) | 1.00§ | 73.6% (39) | 80.4% (45) | 0.59§ | 80.0% (44) | 74.1% (40) | 0.77§ |
| Age (y) | 45.6 (36.1–55.0) | 41.0 (30.0–59.0) | 0.69‡ | 38.0 (36.1–56.1) | 48.0 (30.0–59.0) | 0.96‡ | 38.4 (32.0–52.2) | 48.5 (30.0–59.0) | 0.14‡ |
| Diabetes duration (y) | 26.0 (15.0–39.0) | 27.0 (17.0–39.0) | 0.60‡ | 26.0 (15.0–35.0) | 28.5 (17.0–42.0) | 0.09‡ | 19.0 (17.0–32.0) | 34.5 (17.0–39.0) | **0.03‡** |
| Longest dimension of MA (μm)* | 104.6 (75.9–129.1) | 50.0 (38.3–65.2) | **<0.0001‡** | 86.5 (59.2–119.0) | 48.5 (335.1–65.6) | **<0.0001§** | - | - | - |
| Retinal subfield volume ($mm^3$)† | 0.54 (0.46–1.52) | 0.57 (0.53–1.52) | 0.06‡ | 0.55 (0.47–1.52) | 0.57 (0.54–1.50) | 0.18§ | 0.56 (0.51–1.52) | 0.56 (0.53–1.50) | 0.71‡ |
| Intraluminal hyperreflectivity* | 82.4% (28) | 33.3% (25) | **<0.0001§** | - | - | - | 30.9% (17) | 66.7% (36) | **<0.0003§** |
| MA perfusion* | 76.5% (26) | 33.3% (50) | **<0.0001§** | 79.3% (42) | 16.1% (9) | **<0.0001§** | 25.5% (14) | 68.5% (37) | **<0.0001§** |
| Intraretinal cysts > 250 μm† | 19.2% (5) | 20.0% (11) | 1.0 § | 22.2% (8) | 17.8% (8) | 0.78§ | 27.3 (9) | 14.6% (7) | 0.17§ |
| Hyperreflective foci† | 70.6% (24) | 58.7% (44) | 0.29§ | 71.7% (38) | 53.6% (30) | 0.07§ | 56.4% (31) | 68.5% (37) | 0.24§ |
| MA ring sign† | 60.0% (15) | 39.3% (11) | 0.17§ | 54.1% (20) | 37.5% (6) | 0.37§ | 20.0% (3) | 60.5% (23) | **0.01§** |
| Disorganization of retinal inner layers† | 14.7% (5) | 2.7% (2) | **0.03§** | 9.4% (5) | 3.6% (2) | 0.26§ | 3.6% (2) | 9.3% (5) | 0.27§ |
| Wall deformability* | 25.0% (2) | 16.7% (5) | 0.62§ | 25.0% (5) | 11.1% (2) | 0.41§ | 12.9% (4) | 42.9% (3) | 0.10§ |
| Visibility on fundus photo | 93.2% (28) | 59.1% (39) | **0.001§** | 95.9% (47) | 42.6% (20) | **<0.0001§** | 49.0% (25) | 93.3% (42) | **<0.0001§** |

Bolded values indicate statistical significance, $P < 0.05$. *n*, absolute number.

* Assessed on AOSLO.

† Assessed on SDOCT.

‡ Wilcoxon 2-sample / Kruskal-Wallis test.

§ Fisher's exact test.

yet to be determined. This cross-sectional study does not reveal whether MA WH causes DRIL or whether both findings are caused by other physiologic and/or structural aspects of MAs related to leakage.

Intraluminal hyperreflectivity of MAs on AOSLO was significantly associated with perfusion status and visibility on fundus photography. In these cases, dynamic observation of the MAs during AOSLO imaging suggested that IH was consistent with the presence of blood cell clotting within the MA as described previously.[36,37] IH showed a rough appearance, suggesting a conglomerate of clotted blood cells, and either filled the entire cavity of the respective MA or was connected to the MA wall with adjacent blood cell flow near the IH. Given that later stage MAs are characterized by a loss of endothelial cells, the formation of intraluminal clots may be facilitated by the exposed basement membrane and lack of anticoagulatory factors that normally are secreted by endothelial cells. It is important to note, however, that the finding of IH on some images also theoretically could result from lensing artifacts due to the nature of AOSLO imaging. Lensing artifacts would most likely be caused by the dome-shaped architecture of MAs, and these artifacts are seen commonly as small, bright, and smooth intraluminal hyperreflectivities in the center of an MA lumen. On AOSLO videos, smooth blood flow often is visible within the MA in images focused immediately posterior to these artifacts. In contrast, IH caused by aggregates of blood cells had a rougher appearance and often was adjacent to MA walls. On videos, blood flow around the IH seemed more turbulent. For the purposes of this study, only IH with rough appearance and/or connection to the MA wall was included in the IH analysis.

The combination of high resolution AOSLO imaging and OCT offers new insight in the morphology and structure of MAs in the human eye in vivo. Limitations of this study include the cross-sectional design and limited number of MAs and eyes. Thus, we cannot draw conclusions regarding the relative timing of neural retinal pathology onset in relation to the development of AOSLO MA wall characteristics. The relationship between VA and AOSLO characteristics is based on a small subset of MAs that were centrally located. Furthermore, bias resulting from selective imaging of MAs from eyes of cooperative subjects with clear media could decrease the generalizability of these results. Thus, these findings will need to be validated in larger studies. Additional studies are underway to address longitudinal assessment of MA changes in a larger cohort as well as to determine the correlation of AOSLO MA findings with fluorescein leakage on angiography. Although the transverse resolution of adaptive optics imaging systems is the highest in vivo retinal imaging approach currently available, it remains challenging to reliably resolve details differentiating certain cell types, such as pericytes or endothelial cells. Our AOSLO system's theoretical resolution of approximately 2.5 μm should enable cellular imaging; however, the lack of contrast between adjacent cells is a limiting factor. Advanced imaging setups, such as AOSLO fluorescein angiography, offset aperture AOSLO imaging, rapidly configurable aperture AOSLO imaging, or AO-OCT imaging, may eventually address insufficient tissue contrast.[14,19,21,22,38–41] Furthermore, the combination with OCT-angiography may overcome limitations of both imaging modalities. While OCT-angiography lacks the ability to image non- or little perfused MAs, AOSLO can easily detect such.[42,43] At the same time OCT-angiography is capable of detecting the exact axial location of MAs in relation to the retinal capillary plexuses.

In summary, qualities, such as wall and intraluminal hyperreflectivity as seen on AOSLO, are new variables for the in vivo characterization of microaneurysms and correlate with changes in neural organization that are associated with VA

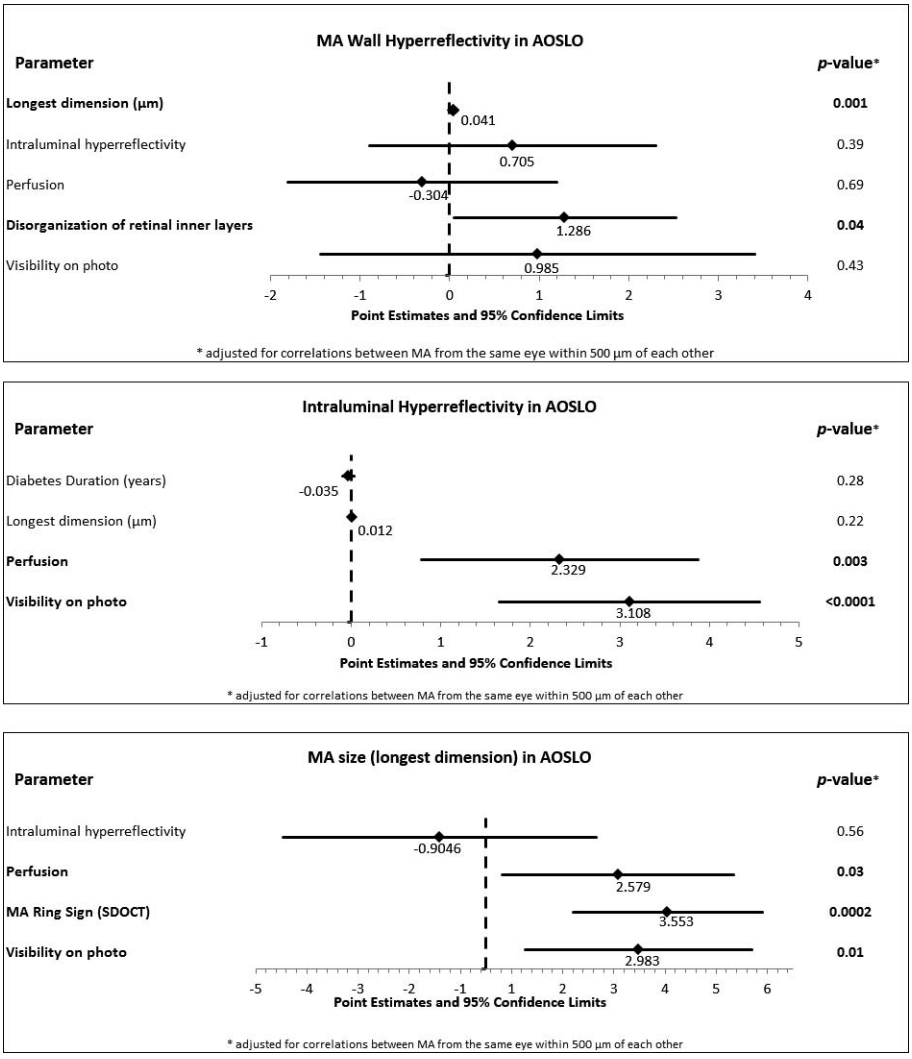


FIGURE 3. Forest plots reporting the point estimates and 95% confidence intervals of multivariable models for wall hyperreflectivity of MA (*top*), IH of MA (*middle*), and MA size (*bottom*). All variables significantly associated in the respective unadjusted analyses were included in creating each of the models. Analyses and *P* values were adjusted for correlations between MAs from the same eye within 500 μm of each other.

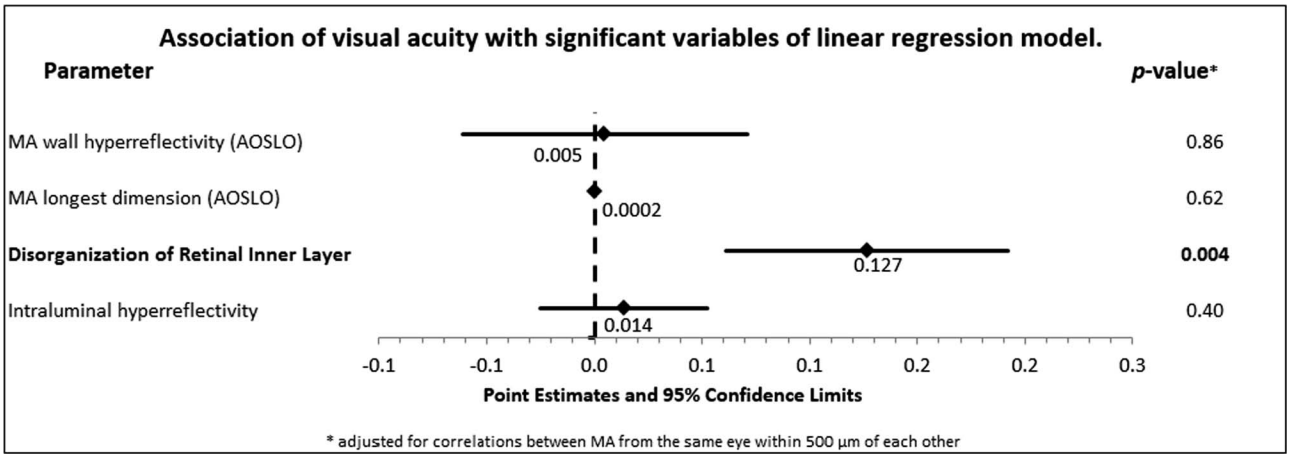


FIGURE 4. Forest plots reporting the point estimates and 95% confidence intervals of multivariable models for visual acuity in the subgroup of MA located within 500 μm of the foveal center. Variables significantly associated in the respective unadjusted analyses were included in creating each of the models. Analyses and *P* values were adjusted for correlations between MAs from the same eye within 500 μm of each other.

outcomes. Wall hyperreflectivity of MAs within the foveal center together with DRIL on SDOCT appear to be new markers associated with VA in patients with DR. Future studies will explore and elucidate longitudinal associations of AOSLO MA characteristics and onset, worsening, or improvement of local neural retinal pathology and visual function over time.

## *Acknowledgments*

The authors thank the study coordinators, Hanna Kwak, Peggy Stockman, and Ann Kopple (Beetham Eye Institute, Boston, MA, USA) for helping with patient recruitment and administrative support.

Supported by National Eye Institute (NEI; Bethesda, MD, USA) Grants R01 EY024702, R44 EY016295, and P30EY019008; JDRF 3-SRA-2014-264-M-R, and 17-2011-359; Eleanor Chesterman Beatson Childcare Ambassador Program Foundation Grant; NIDDK 5 P30 DK036836-24 P&F Grant; Massachusetts Lion Eye Research Fund Inc.; and Boston Micromachines.

Disclosure: **J. Lammer**, None; **S.G. Karst**, None; **M.M. Lin**, None; **M. Cheney**, None; **P.S. Silva**, Boston Micromachines (C); **S.A. Burns**, None; **L.P. Aiello**, Boston Micromachines (C); **J.K. Sun**, Boston Micromachines (C)

## *References*

1. Early Treatment Diabetic Retinopathy Study Research Group. Grading diabetic retinopathy from stereoscopic color fundus photographs: an extension of the modified Airlie house classification. ETDRS Report Number 10. *Ophthalmology*. 1991;98:786–806.
2. Klein R, Meuer SM, Moss SE, Klein BEK. The relationship of retinal microaneurysm counts to the 4-year progression of diabetic retinopathy. *Arch Ophthalmol*. 1989;107:1780–1785.
3. Ribeiro ML, Nunes SG, Cunha-Vaz JG. Microaneurysm turnover at the macula predicts risk of development of clinically significant macular edema in persons with mild nonproliferative diabetic retinopathy. *Diabetes Care*. 2013; 36:1254–1259.
4. Yanoff M. Diabetic retinopathy. *N Engl J Med*. 1966;274: 1344–1349.
5. Stitt AW, Gardiner TA, Archer DB. Histological and ultrastructural investigation of retinal microaneurysm development in diabetic patients. *Br J Ophthalmol*. 1995;79:362–367.
6. Fryczkowski AW, Chambers RB, Craig EJ, Walker J, Davidorf FH. Scanning electron microscopic study of microaneurysms in the diabetic retina. *Ann Ophthalmol*. 1991;23:130–136.
7. Hammes H-P, Lin J, Renner O, et al. Pericytes and the pathogenesis of diabetic retinopathy. *Diabetes*. 2002;51: 3107–3112.
8. Hammes H-P. Pericytes and the pathogenesis of diabetic retinopathy. *Horm Metab Res*. 2005;37(suppl 1):39–43.
9. Liang J, Williams DR, Miller DT. Supernormal vision and high-resolution retinal imaging through adaptive optics. *J Opt Soc Am A Opt Image Sci Vis*. 1997;14:2884–2892.
10. Roorda A, Romero-Borja F, Donnelly W III, Queener H, Hebert T, Campbell M. Adaptive optics scanning laser ophthalmoscopy. *Opt Express* 2002;10:405–412.
11. Zhang Y, Poonja S, Roorda A. MEMS-based adaptive optics scanning laser ophthalmoscopy. *Opt Lett*. 2006;31:1268–1270.
12. Zhong Z, Petrig BL, Qi X, Burns SA. In vivo measurement of erythrocyte velocity and retinal blood flow using adaptive optics scanning laser ophthalmoscopy. *Opt Express*. 2008;16: 12746–12756.
13. Zhong Z, Song H, Chui TYP, Petrig BL, Burns SA. Noninvasive measurements and analysis of blood velocity profiles in human retinal vessels. *Invest Ophthalmol Vis Sci*. 2011;52: 4151–4157.
14. Chui TYP, Mo S, Krawitz B, et al. Human retinal microvascular imaging using adaptive optics scanning light ophthalmoscopy. *Int J Retin Vitr*. 2016;2:11.
15. Karst SG, Lammer J, Radwan S, et al. Characterization of In vivo retinal lesions of diabetic retinopathy using adaptive optics scanning laser ophthalmoscopy. *Int J Endocrinol*. 2018;2018:7492946.
16. Arichika S, Uji A, Hangai M, Ooto S, Yoshimura N. Noninvasive and direct monitoring of erythrocyte aggregates in human retinal microvasculature using adaptive optics scanning laser ophthalmoscopy. *Invest Ophthalmol Vis Sci*. 2013;54:4394–4402.
17. Lombardo M, Parravano M, Serrao S, Ducoli P, Stirpe M, Lombardo G. Analysis of retinal capillaries in patients with type 1 diabetes and nonproliferative diabetic retinopathy using adaptive optics imaging. *Retina*. 2013;8:1630–1639.
18. Pinhas A, Dubow M, Shah N, et al. In vivo imaging of human retinal microvasculature using adaptive optics scanning light ophthalmoscope fluorescein angiography. *Biomed Opt Express*. 2013;4:1305.
19. Dubow M, Pinhas A, Shah N, et al. Classification of human retinal microaneurysms using adaptive optics scanning light ophthalmoscope fluorescein angiography. *Invest Ophthalmol Vis Sci*. 2014;55:1299–1309.
20. Burns SA, Elsner AE, Chui TY, et al. In vivo adaptive optics microvascular imaging in diabetic patients without clinically severe diabetic retinopathy. *Biomed Opt Express*. 2014;5: 961–974.
21. Pinhas A, Razeen M, Dubow M, et al. Assessment of perfused foveal microvascular density and identification of nonperfused capillaries in healthy and vasculopathic eyes. *Invest Ophthalmol Vis Sci*. 2014;55:8056–8066.
22. Mo S, Krawitz B, Efstathiadis E, et al. Imaging foveal microvasculature: optical coherence tomography angiography versus adaptive optics scanning light ophthalmoscope fluorescein angiography. *Invest Ophthalmol Vis Sci*. 2016;57: OCT130–OCT140.
23. Lu Y, Bernabeu MO, Lammer J, et al. Computational fluid dynamics assisted characterization of parafoveal hemodynamics in normal and diabetic eyes using adaptive optics scanning laser ophthalmoscopy. *Biomed Opt Express*. 2016;7:4958.
24. Geitzenauer W, Hitzenberger CK, Schmidt-Erfurth UM. Retinal optical coherence tomography: past, present and future perspectives. *Br J Ophthalmol*. 2011;95:171–177.
25. Horii T, Murakami T, Nishijima K, Sakamoto A, Ota M, Yoshimura N. Optical coherence tomographic characteristics of microaneurysms in diabetic retinopathy. *Am J Ophthalmol*. 2010;150:840–848.
26. Wang H, Chhablani J, Freeman WR, et al. Characterization of diabetic microaneurysms by simultaneous fluorescein angiography and spectral-domain optical coherence tomography. *Am J Ophthalmol*. 2012;153:861–867.e1.
27. Early Treatment Diabetic Retinopathy Study Research Group. Fundus photographic risk factors for progression of diabetic retinopathy. ETDRS Report number 12. *Ophthalmology*. 1991;98(suppl 5):823–833.
28. Webb RH, Albanese MJ, Burns SA. Stroke amplifier for deformable mirrors. *Appl Opt*. 2010;43:5330–5333.
29. Burns SA, Elsner AE, Ferguson D, Hammer DX. Large-field-of-view, modular, stabilized, adaptive-optics-based scanning laser ophthalmoscope. *J Opt Soc Am A Opt Image Sci Vis*. 2007;24: 1313–1326.
30. Lammer J, Prager SG, Cheney MC, et al. Cone photoreceptor irregularity on adaptive optics scanning laser ophthalmoscopy correlates with severity of diabetic retinopathy and

macular edema. *Invest Opthalmol Vis Sci*. 2016;57:6624–6632.

31. Microsoft Corporation. WAVE and AVI codec registries - RFC 2361. *IETF*. 1998;06.
32. Schindelin J, Arganda-Carreras I, Frise E, et al. Fiji: an open-source platform for biological-image analysis. *Nat Methods*. 2012;9:676–682.
33. Sun JK, Lin MM, Lammer J, et al. Disorganization of the retinal inner layers as a predictor of visual acuity in eyes with center-involved diabetic macular edema. *JAMA Ophthalmol*. 2014;132:1309–1316.
34. Vujosevic S, Bini S, Torresin T, et al. Hyperreflective retinal spots in norma and diabetic eyes: B-scan and en face spectral domain optical coherence tomography evaluation. *Retina*. 2017;37:1092–1103.
35. Sun JK, Radwan SH, Soliman AZ, et al. Neural retinal disorganization as a robust marker of visual acuity in current and resolved diabetic macular edema. *Diabetes*. 2015;64:2560–2570.
36. Tam J, Dhamdhere KP, Tiruveedhula P, et al. Disruption of the retinal parafoveal capillary network in type 2 diabetes before the onset of diabetic retinopathy. *Invest Ophthalmol Vis Sci*. 2011;52:9257–9266.
37. Karst SG, Salas M, Hafner J, et al. Three-dimensional analysis of retinal microaneurysms with adaptive optics optical coherence tomography [published online ahead of print January 19, 2018]. *Retina*. doi:10.1097/IAE.0000000000002037.
38. Chui TYP, Gast TJ, Burns SA. Imaging of vascular wall fine structure in the human retina using adaptive optics scanning laser ophthalmoscopy. *Invest Ophthalmol Vis Sci*. 2013;54:7115–7124.
39. Chui TYP, Pinhas A, Gan A, et al. Longitudinal imaging of microvascular remodelling in proliferative diabetic retinopathy using adaptive optics scanning light ophthalmoscopy. *Ophthalmic Physiol. Opt*. 2016;36:290–302.
40. Scoles D, Sulai YN, Langlo CS, et al. In vivo imaging of human cone photoreceptor inner segments. *Invest Ophthalmol Vis Sci*. 2014;55:4244–4251.
41. Sapoznik KA, Luo T, de Castro A, et al. Enhanced retinal vasculature imaging with a rapidly configurable aperture. *Biomed Opt Express*. 2018;9:1323–1333.
42. Parravano M, De Geronimo D, Scarinci F, et al. Diabetic microaneurysms internal reflectivity on spectral-domain optical coherence tomography and optical coherence tomography angiography detection. *Am J Ophthalmol*. 2017;179:90–96.
43. Hamada M, Ohkoshi K, Inagaki K, Ebihara N, Murakami A. Visualization of microaneurysms using optical coherence tomography angiography: comparison of OCTA en face, OCT B-scan, OCT en face, FA, and IA images. *Jpn J Ophthalmol*. 2018;62:176–178.

Investigative Ophthalmology & Visual Science